Dyes and Pigments 91 (2011) 126–133

Contents lists available at ScienceDirect

Dyes and Pigments

journal homepage: www.elsevier.com/locate/dyepig

The mechanism for the colour change of iron chromium black pigments in glazes through transmission electron microscopy techniques

Hilmi Yurdakul, Servet Turan*, Emel Ozel

Department of Materials Science and Engineering, Anadolu University (AU), Iki Eylul Campus, 26480 Eskisehir, Turkey

ARTICLE INFO

Article history:
Received 19 December 2010
Received in revised form
7 March 2011
Accepted 9 March 2011
Available online 2 April 2011

Keywords:
Fe–Cr black pigment
Glaze
Transmission electron microscopy (TEM)
Electron energy loss spectroscopy (EELS)
Energy dispersive X-ray spectroscopy (EDXS)
Focused ion beam (FIB)

ABSTRACT

Black iron–chromium (Fe–Cr) bearing oxide pigments are generally utilised as effective colourants in a wide variety of applications. However, in the case of their use within ZnO-containing glazes, they yield an undesirable *brown colour* instead of expected black colour. In order to understand the colour change in this system, we report the use of focused ion beam (FIB) sample preparation technique followed by the use of analytical transmission electron microscopy (TEM) characterisation techniques. According to the results, the formation of a reaction layer between the pigment and glaze was identified with an average composition of $Zn_{0.48}Fe_{0.79}Cr_{1.32}O_4$. Additionally, the valance of Fe was determined as 3+ in the pigment grain, whereas 2+ in the reaction layer and the glaze, respectively. Therefore, it was concluded that the colour change is occurring as result of the valence variation of Fe, the formation of $Zn_{0.48}Fe_{0.79}Cr_{1.32}O_4$ compound and the outward diffusion of Fe into the glaze.

1. Introduction

Inorganic black pigments are extensively used to satisfy a wide range of requirements for different industrial applications e.g., as a starting raw materials in body formulations of porcelain tiles and sanitary wares, as well as in glaze compositions [1–3]. Therefore, recent consumption of these pigments has been considerably increasing as a result of rising demands together with aesthetic concerns in the ceramic industries [1,3]. Moreover, around twenty-five percent of the utilisation in the market belongs to the inorganic black pigments. This is why there is a scientific and industrial interest on this material [1,3].

Fe–Cr oxide containing black pigments can be commonly produced from a mixture of pure Cr_2O_3 (chromium (3+) oxide) and Fe_2O_3 (iron (3+) oxide) in a proportion by weight with assistance of heat treatment over 1100 °C [4,5]. In addition to this conventional route, Fe–Cr pigments can also be synthesised from secondary raw materials and waste resources [3,6]. However, a widespread use of a particular pigment is also mainly determined by their crystal structure characteristics that govern the colouring power. Fe–Cr pigments can primarily be in two different crystal structures: (i) corundum and (ii) spinel [7–11]. The black Fe–Cr oxide pigments are structurally a substitutional solid solution with the corundum-type crystal lattice [7,8]. On the other hand, these pigments are also found in $Fe_{1+y}Cr_{2-y}O_4$ spinel structure type [9–11]. The spinel structure type can involve both divalent and trivalent Fe ions in its crystal structure [12]. In this case, the variable oxidation state of Fe can further lead to instabilities on controlling the colouring effect of pigments, since it is well-known that iron gives different colours in its 2+ and 3+ states [13].

Colouring performance of ceramic pigments not only depends on the nature of crystal structure, but also it is intensely affected by possible reactions evolving when they are introduced within ceramic-matrices, e.g., in the glazes and frits [14–17]. The reasons of these unavoidable reactions are most likely due to the dissolution of pigment and/or glaze through chemical attacks during firing [18,19]. Therefore, a few studies tried to focus on this issue in various pigment-glaze/frit systems [14–17]. However, the main challenge is still to understand the possible interactions occurring between pigments and ceramic-matrices resulting in a colour change after firing. An XRD based study [20] intended to explain this phenomenon and showed that ZnO-iron-chromium spinel formation could be the main reason of this problem. Afterwards, an explicit reaction layer formation between Fe–Cr pigment and Zn-based glaze was visually detected and its chemical composition was qualitatively demonstrated using a combination of scanning electron microscopy (SEM) and energy dispersive X-ray (EDX) spectroscopy analysis [4]. However, due to the large spatial

* Corresponding author. Tel.: +90 222 3213550x6356; fax: +90 222 3239501.
E-mail address: sturan@anadolu.edu.tr (S. Turan).

0143-7208/$ – see front matter © 2011 Elsevier Ltd. All rights reserved.
doi:10.1016/j.dyepig.2011.03.014

Table 1
The composition of pigment powder and glaze used in the current study (wt.%).

	Na_2O	K_2O	MgO	CaO	SiO_2	Al_2O_3	ZnO	Fe_2O_3	Cr_2O_3
Pigment	–	–	–	0.1	0.6	0.3	–	64.3	34.7
Glaze	2.9	3.0	1.2	11.2	63.5	9.1	9.1	–	–

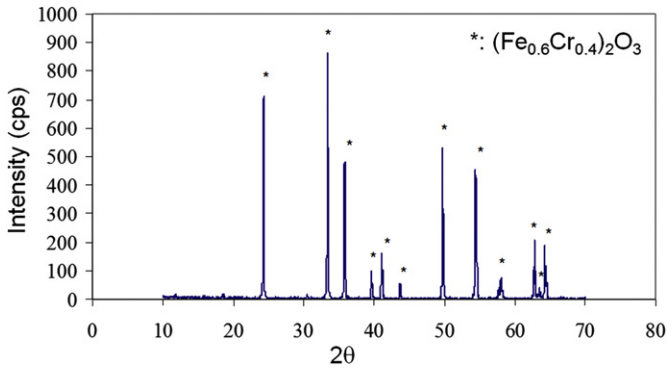

Fig. 1. XRD pattern of Fe–Cr black pigment powder calcined at 1250 °C.

resolution limit of EDX in SEM, the exact composition of this reaction layer was not precisely identified. Although this can be achieved by using TEM based chemical analysis techniques, the use of TEM techniques to clarify these issues has not been undertaken until recently due to the difficulties in sample preparation of brittle materials like thin glazes covering a ceramic body. However, now a new sample preparation method called focused ion beam (FIB) technique is available to prepare a sample from any chosen interface between a pigment grain and an interaction layer from the sample. For such a purpose, in a very recent study [14], a TEM sample from the pigment-glassy coating interface in the case of Co-doped willemite ceramic pigments was successfully prepared with FIB technique and analytical TEM analyses were carried out to clear whether any diffusion arises in this system or not. Similarly, analytical TEM analyses of an electron-transparent sample prepared from the reaction layer formed between Fe–Cr black pigment and ZnO-containing glaze with the practice of FIB technique could also bring some light to reveal the mechanism for the colour change occurring in this system.

Therefore, the objective of this research is to determine the precise chemistry of the reaction layer formed between Fe–Cr black pigment and ZnO-containing glaze by using analytical TEM based techniques on FIB prepared samples to understand the mechanism for the colour change.

2. Materials and methods

2.1. Production and characterisation of pigment

60 wt.% Cr_2O_3 (Merck) and 40 wt.% Fe_2O_3 (Merck) powders were mixed and ground with water in a ball mill for 3 h to obtain homogeneous slurries. Afterwards, the slurries were dried at 100 °C and calcined in an electric furnace at 1250 °C for 3 h by applying a heating rate of 2 °C/min. Then, 3 wt.% Fe–Cr black pigment containing deliberately selected large particles was introduced into a ZnO-containing transparent glaze (Table 1), and applied to an engobed single firing ceramic tile body. Finally, the colour-glazed ceramic tile substrates were fired at 1125 °C for 45 min.

The chemical composition of pigment powder after calcination was determined by using X-ray fluorescence spectrometer (XRF, Rigaku RZS Primus) whereas the crystalline phases in the pigment powder after calcination were determined by using X-ray diffraction (XRD, Rigaku, d/max 2000) analysis.

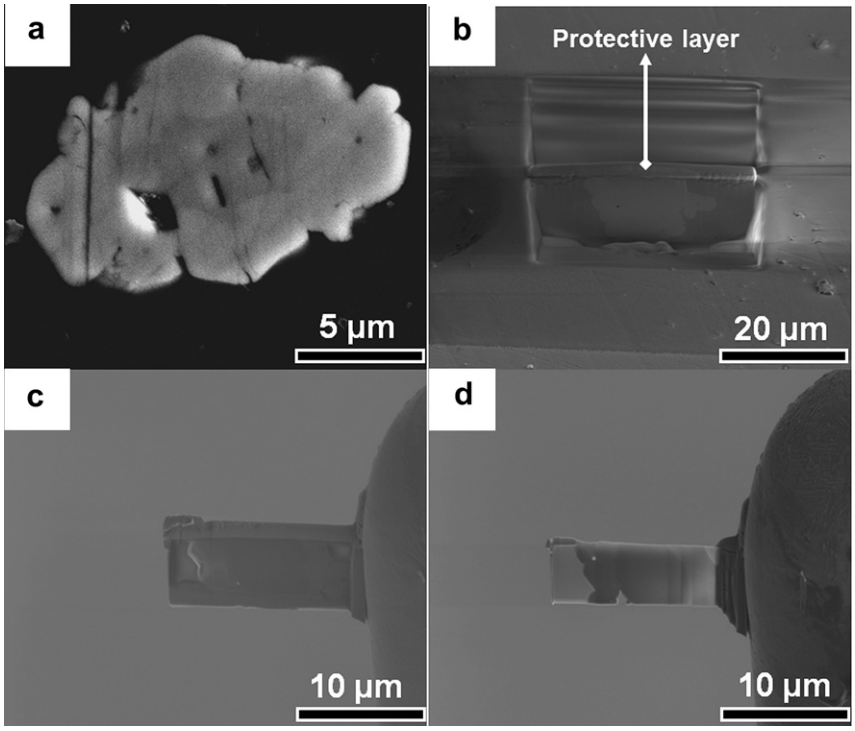

Fig. 2. (a) Back scattered SEM image of an embedded pigment grain in the glaze. Note that the black contrast at core of pigment grain indicates the remaining Fe–Cr pigment after firing, whereas white-contrast surrounding the core shows the formation of reaction layer. (b–d) SEM images demonstrating the steps of FIB sample preparation process: (b) selecting the site of interest including pigment, reaction layer and glaze, and milling from the both sides of the protection layer, (c) after cutting and lifting out the TEM sample before further thinning and (d) thinned sample ready for the investigations.

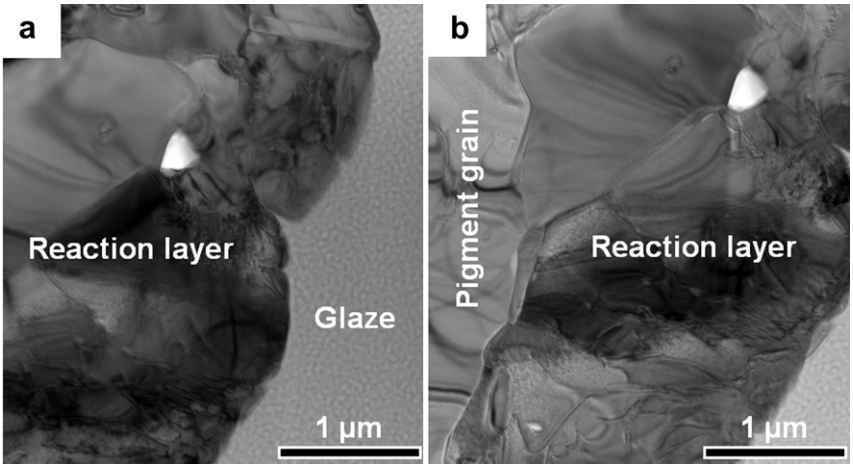

Fig. 3. (a and b) Bright field (BF) TEM images signifying the glaze, pigment and reaction layer regions.

2.2. TEM sample preparation with FIB technique

Electron-transparent samples for TEM investigations from the colour-glazed ceramic tile substrates were prepared by using the combination of focused ion beam (FIB)-scanning electron microscope (SEM) system (FEI-Nova 600 NanoLab DualBeam™). This combination can provide a selection of interfaces that formed between Fe–Cr pigment and the ZnO-containing glaze. But, before starting the thinning process in FIB, the large size pigment grains were preferentially chosen by means of SEM imaging, because they include large interfaces and still keep unreacted part of a pigment grain to understand the changes in a pigment grain embedded in a glaze after firing.

2.3. Transmission electron microscopy (TEM) studies

FIBed sample was characterised by using a field emission TEM (Jeol 2100F), operating at 200 kV and equipped with an energy filter (Gatan GIF Tridiem), parallel electron energy loss spectrometer (EELS), a high angle annular dark field scanning transmission electron microscope (HAADF-STEM) detector (Fishione), annular dark field (ADF) detector and an energy dispersive X-ray (EDX) spectrometer (Jeol JED-2300T). In STEM-based EDX and EELS chemical analyses, an electron spot with 1–2 nm in diameter was used. Furthermore, a drift corrector was used to avoid any possible drifts that may occur at nano-scale during the acquisition of STEM-EDX/EELS analyses. During EDX analysis, STEM mode was preferred instead of TEM mode due to the fact that the spatial resolution of EDX in STEM is smaller (only a few nm) and elemental mapping can only be done in a STEM-EDX combination [21]. In STEM-based EELS analysis, the convergence and collection semi-angles were used as 9.2 and 15.7 mrad, respectively. The spectrometer energy dispersions were also chosen in 0.2 and 0.5 eV/channels. The backgrounds in EELS analyses were subtracted according to power-law [22]. For quantitative EELS analysis, the partial inelastic cross-sections were derived from Hartree–Slater model [22], and the calculations were based on the relative quantification method [22]. The thickness of the FIBed sample was also calculated by using the EELS with absolute log-ratio method [22].

3. Results and discussion

3.1. Characterisation of pigments

XRD analysis of Fe–Cr pigment powder calcined at 1250 °C showed that the pigment only contains $(Fe_{0.6}Cr_{0.4})_2O_3$ [JPDS card no: 00-034-0412] phase (Fig. 1). This result also elucidated that Fe_2O_3 and Cr_2O_3 constituted as a solid solution in corundum structure. Additionally, the chemical analysis of pigment powder after calcination determined that pigment was composed of

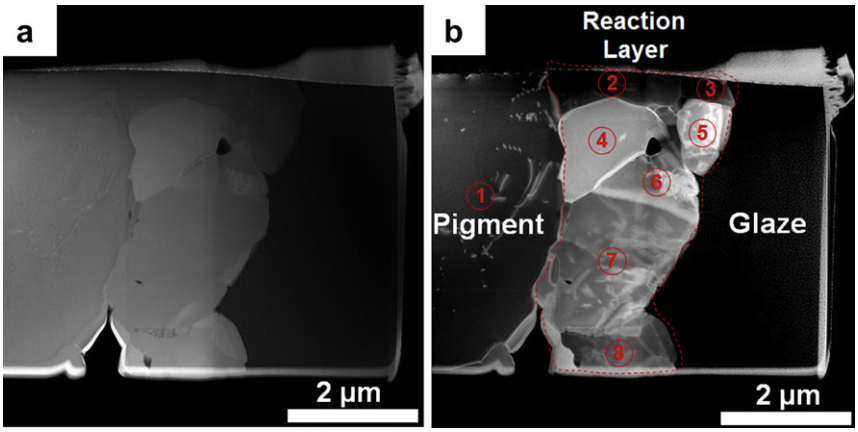

Fig. 4. (a) STEM-HAADF and (b) STEM-ADF images depicting the pigment, reaction layer and glaze regions. Please note that the numbers on the STEM-ADF image correspond to the individual grains in the reaction layer (also marked with dashed line).

approximately 64.3 wt.% Fe_2O_3 and 34.7 wt.% Cr_2O_3 (Table 1), which corresponds to $(Fe_{0.635}Cr_{0.365})_2O_3$ in atomic composition. This data together with the assistance of XRF analysis also revealed that it was consistent with the starting pigment composition (60 wt.% Fe_2O_3 and 40 wt.% Cr_2O_3 equalling to $(Fe_{0.585}Cr_{0.415})_2O_3$ atomic formulation) and with the crystallographic composition $(Fe_{0.6}Cr_{0.4})_2O_3$ determined from XRD analysis (Fig. 1). However, when the starting pigment composition, XRD and XRF analyses are considered together, it can be said that a minor amount of chromium (Cr) loss might occur during the production of Fe–Cr black pigments at 1250 °C due to the higher volatilisation of Cr in comparison to Fe [7].

3.2. Observations during the FIB sample preparation

The SEM image series in Fig. 2 demonstrate the progressive steps of FIB sample preparation route for analytical TEM investigations. A specific region covering the whole of Fe–Cr pigment grain, reaction layer and glaze was selected (Fig. 2(a)) and covered with protective platinum (Pt) layer and the sample surface was bombarded with gallium (Ga) ions from both sides of the protective layer (Fig. 2(b)). Afterwards, the sample was cut from sides and bottom end and lifted out for further thinning (Fig. 2(c)). After thinning, it can be seen that the size of the specimen is approximately 12 μm (length) × 6 μm (width) (Fig. 2(d)). More importantly, it should be noted that the thickness of sample was calculated to be around 75 nm by using EELS analysis. This means that FIBed specimen is thin enough to avoid underneath grain effect that might cause misleading results during chemical analysis [23].

3.3. TEM imaging and chemical analyses of FIBed sample

Bright field (BF) TEM images showed the formation of a reaction layer between the Fe–Cr pigment and ZnO-containing glaze after firing (Fig. 3). These images also point out that the reaction layer is composed of grains rather than a continuous homogenous layer, while the ZnO-containing glaze matrix was completely vitrified at 1125 °C.

The STEM images in Fig. 4 also consolidate the first results obtained with the TEM-BF images. The achievable image intensity in STEM-HAADF imaging technique is approximately proportional to the square of the atomic number (Z), which means that regions containing higher atomic number elements would appear brighter in the microstructure [24]. Therefore, in the Z-contrast HAADF-STEM image (Fig. 4(a)), the vitrified ZnO-containing glaze consisting of lower atomic number elements can be visualised as almost black whereas higher atomic number elements containing Fe–Cr pigment grain and the reaction layer could be seen as grey regions, respectively, in contrast to the TEM-BF images given in Fig. 3. A distinct contrast between pigment and glaze regions highlighted with dashed-lines can also be seen in an ADF image (Fig. 4(b)), clearly indicating the formation of a reaction layer composed of individual grains marked with numbers between 2 and 8.

Since the position of the reaction layer is well-defined, the representative chemical compositions of the glaze, pigment grain and reaction layer can be determined by using energy dispersive X-ray (EDX) point analysis (Fig. 5(a–c)). Furthermore, to visually show the distribution of elements detected during the EDX point analyses (Fig. 5(a–c)), the EDX mapping was also acquired from Zn-K_α (8.6 keV), Fe-K_α (6.4 keV), Cr-K_α (5.4 keV), Ca-K_α (3.7 keV), Si-K_α (1.7 keV) and O-K_α (0.5 keV) characteristic X-ray lines to avoid any possible overlapping problems in the spectrum (Fig. 6). Based on the data in Figs. 5 and 6, it can be deduced that the EDX point and mapping analyses clearly show the reaction layer formation as a result of the diffusion of Fe and Cr from the pigment side and Zn from the glaze side with the help of high temperature (1125 °C). Additionally, the Fe-K_α:Cr-K_α ratio appears to be considerably lower in the reaction layer (≅0.75) in comparison to the pigment grain (≅8.33) suggesting a higher diffusion of Cr than Fe towards the reaction layer. This can also be visually noticed looking in Fig. 6(c and e). On the other hand, the diffusion of Zn from the glaze towards the pigment is much faster than that of Mg and Al. Furthermore, a minor amount of Fe also diffused from the reaction layer into the glaze (Fig. 5(a)). Therefore, at this point, it can be stated that the formation of the reaction layer (containing Fe, Cr, Zn and O elements) and also the diffusion of Fe into the glaze may play an important role on the evolution of brown colour in the glaze. This idea can find a support from a previous study that the

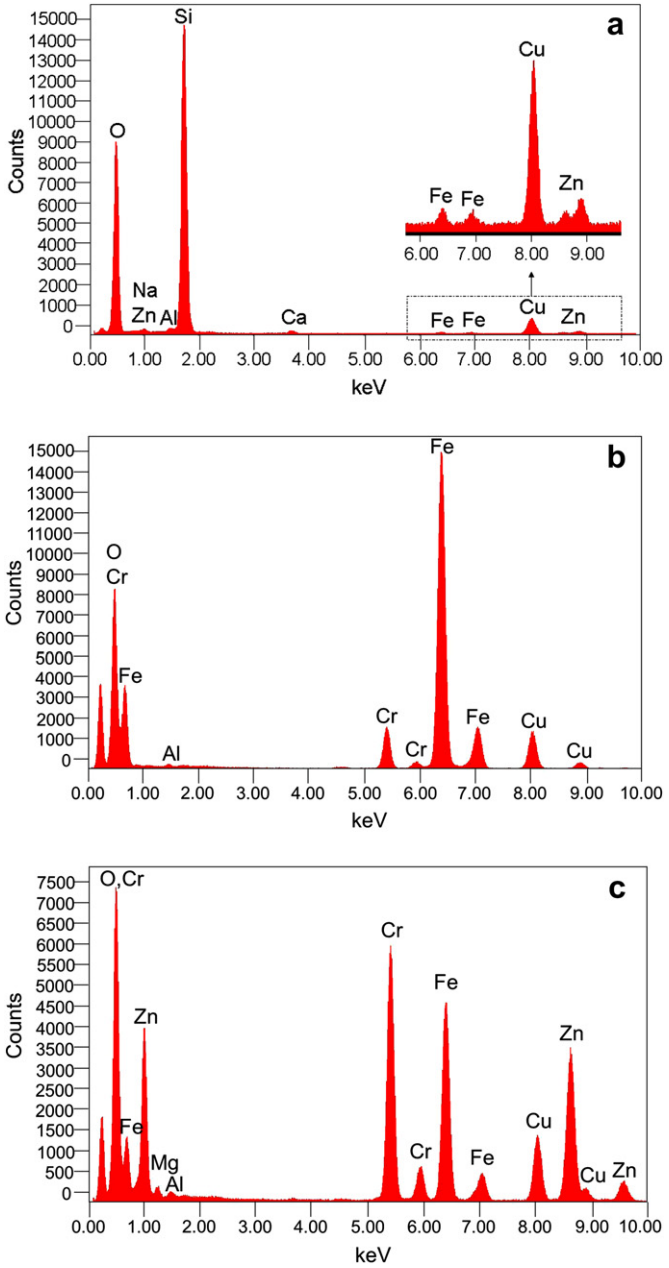

Fig. 5. The STEM-EDX point analyses of (a) the glaze region (the inset image indicates the detailed view of energy range between 6.00 keV and 9.00 keV, marked with dashed line and arrow), (b) the pigment grain and (c) the reaction layer. Please also note that the positions of STEM probe in each analysed points were chosen away from the neighbouring regions to avoid any contributions from the neighbouring grains.

stabilisation of haematite's red colour in glaze could be achieved by preventing outward diffusion of Fe from the pigment crystal [25]. It should also be noted that the obtained STEM-EDX findings were in good agreement with the stabilisation energies of the crystalline field [157.6 kJ/mol for Cr^{3+} (d^3) and 0 for Fe^{3+} (d^5)] in terms of explaining the outward diffusion of Fe and Cr, resulting with the formation of a reaction layer surrounding the pigment grain [26]. Also, it is well-known that compounds which melt at lower temperatures have higher ionic diffusion coefficients than those melting at higher temperatures [27,28]. Hence, this is the clear reason why Zn diffusion from glaze towards the pigment was much faster than Mg and Al in oxide forms.

Despite the fact that chemical constituents of reaction layer were determined by using STEM-EDX based techniques in Figs. 5 and 6, the degree of diffused elements towards the reaction layer should be clarified for accurate quantification of the reaction layer. Therefore, EELS analysis was carried out as a complementary technique to STEM-EDX analysis, since the EEL signals were directly collected with a spectrometer positioned under the sample without causing any fluorescence and absorption effects [22]. Fig. 7 shows EELS analyses of O-K (532 eV), Cr-$L_{3,2}$ (575 eV), Fe-$L_{3,2}$ (708 eV) and Zn-$L_{3,2}$ (1020 eV) edges acquired from the glaze, the pigment grain and the reaction layer, respectively. Based on the results presented in Fig. 7(a–c), at a first glance, it can be easily recognised that Fe diffused into the glaze while Cr and Zn were concentrated in the reaction layer. This observation clearly confirmed the STEM-EDX chemical analyses given in Figs. 5 and 6. Thus, we can strongly claim that Zn diffused towards the pigment side from the amorphous glaze and reacted with the Cr and Fe coming from the pigment grain to generate a new compound surrounding the black Fe–Cr pigment.

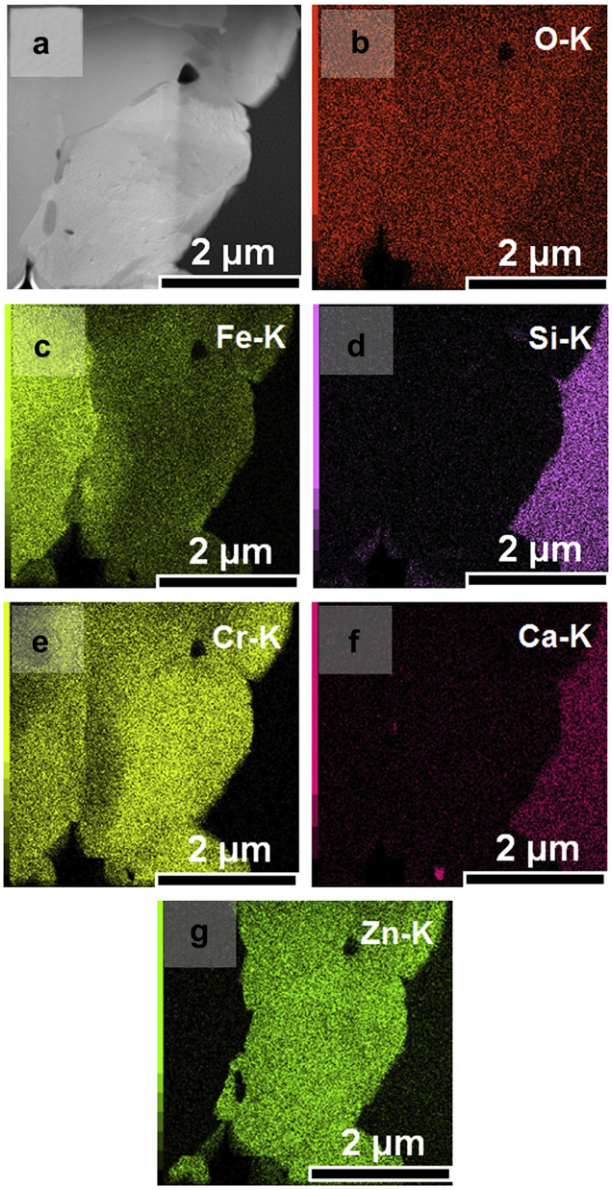

Fig. 6. (a) STEM-HAADF image and (b–g) the X-ray elemental maps of O-K_α, Fe-K_α, Si-K_α, Cr-K_α, Ca-K_α and Zn-K_α characteristic lines, respectively.

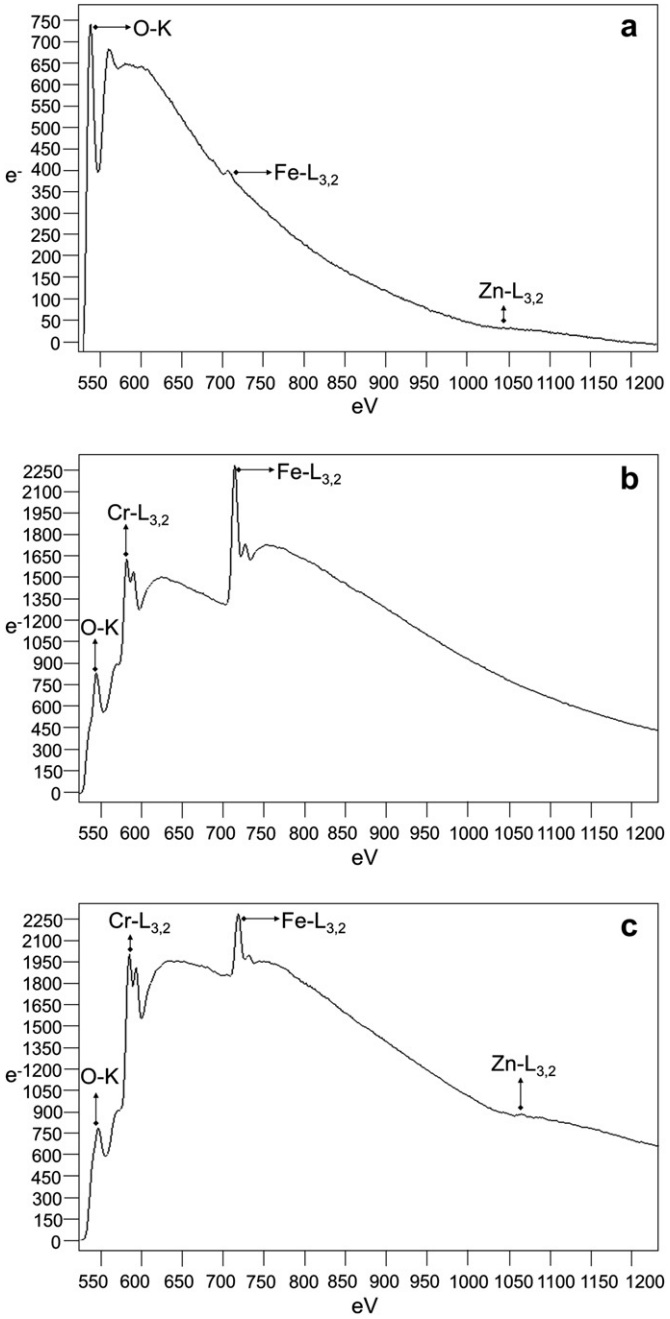

Fig. 7. The EEL spectra obtained from (a) the glaze, (b) the pigment grain and (c) the reaction layer.

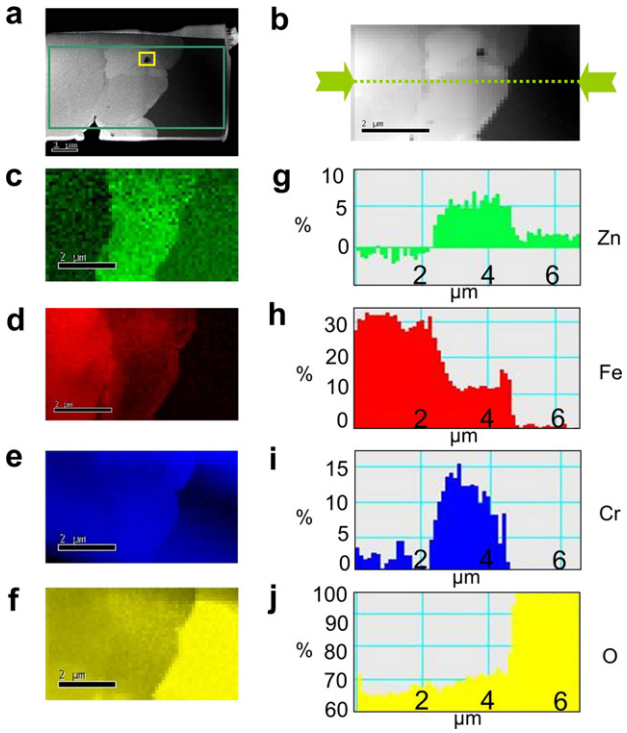

Fig. 8. (a) STEM-HAADF image indicating the rectangular spectrum image area along with the selected spatial drift correction square, (b) the view of STEM-SI (spectrum imaging) after acquisition was completed, (c–f) at % quantitative EELS elemental maps of Zn-$L_{3,2}$, Fe-$L_{3,2}$, Cr-$L_{3,2}$ and O-K edges, respectively, (g–j) % atomic concentration variation of Zn, Fe, Cr and O elements throughout a line labelled with arrows in (b).

For the quantitative analysis of the pigment and the reaction layer by using EELS analysis, STEM-SI (spectrum imaging) [22] data set was first collected from the FIBed sample (Fig. 8(a) and (b)). Afterwards, atomic percentage quantitative EELS elemental maps were subtracted from the STEM-SI data set by using Zn-$L_{3,2}$, Fe-$L_{3,2}$, Cr-$L_{3,2}$ and O-K edges (Fig. 8(c–f)). Finally, atomic concentrations of Zn, Fe, Cr and O elements throughout a line (labelled in Fig. 8(b)) were calculated based on the quantitative EELS elemental maps (Fig. 8(c–f)) and graphically shown in Fig. 8(g–j). By using these results, the chemical compositions of pigment grain and the reaction layer can be easily calculated at a specific distance of the line. For example, at 3 μm, the stoichiometry of the reaction layer is calculated to be $Zn_{0.33}Fe_{0.67}Cr_{0.67}O_4$. Please also note that the composition of any desirable point along the line can be computed from Fig. 8(g–j). Furthermore, for the calculation of average compositions of the pigment and the reaction layer, STEM-SI-EELS spot data from the individual grains composing the reaction layer and pigment (points 1–8 in Fig. 4(a)) were used. The average compositions of pigment and every individual grains in the reaction layer are summarised in Table 2. Here, the results certainly showed that chemical compositions of individual grains existing in reaction layer differed from grain to grain because of the changeable diffusion paths of the Zn, Fe and Cr elements in the system. Therefore, the average composition of the reaction layer was determined as $Zn_{0.48}Fe_{0.79}Cr_{1.32}O_4$ (atomic %). This also indicates a higher diffusion of Cr than Fe from the pigment grain towards the reaction layer and is in well agreement with the qualitative EDX point and mapping analyses (Figs. 5(c) and 6(c and e)). On the other hand, the Fe/Cr ratio in the remnant part of the pigment grain was calculated to be 1.97 which is supporting the results obtained from EDX analysis that outward Cr diffusion is higher than Fe. Since the outward Fe and Cr diffusion from the pigment is different, the composition of the pigment would not be expected to be same as the starting composition given in Table 1.

To find out the oxidation states of Fe after interaction, the EEL spectra for Fe-$L_{3,2}$ edges from the pigment grain, the reaction layer and the glaze were acquired and compared in Fig. 9. In order to see the consistency of valance state in all the grains in the reaction layer, first of all, the EEL spectra for Fe-$L_{3,2}$ edges from each grain in the reaction layer were compared (Fig. 9(a)) and observed that the positions of Fe-L_3 and Fe-L_2 edges for all the grains are similar. Then, from the EEL spectra (Fig. 9(b)), it was also deduced that the positions of Fe-L_3 and Fe-L_2 edges in the reaction layer and the glaze were shifted from the 716 eV and 729 eV corresponding fingerprints of the Fe-L_3 and Fe-L_2 edges in pigment grain towards the 711 eV and 723 eV. As a general rule, the $L_{3,2}$ edges for a specific 3d transition metal exhibit a chemical shift towards higher energy losses with an increase in oxidation state [29]. This characteristic chemical shift was used to determine whether iron is in divalent or trivalent state [30–32]. Hence, in the light of the clear chemical shift observed in the comparative EEL spectra (Fig. 9), we are able to state that the oxidation states of Fe varies from the 3+ state in the pigment grain to 2+ state both in the reaction layer and the glaze.

Although the pure forms of Fe_2O_3 (iron (3+) oxide) and FeO (iron (2+) oxide) are well-known and give the characteristic colours of red and black, respectively, it can be clearly seen that they exhibit different colour in the case of iron in the glaze or glass structures, in comparison to their pure forms [33]. As an example, ferrous iron (Fe^{2+}) produces a blue–green colour in soda-lime-silicate glass, while the same amount of ferric iron (Fe^{3+}) gives a glass that is almost colourless [34]. On the other hand, in other glasses, ferrous iron (Fe^{2+}) brings yellow and pink colours, whereas ferric iron (Fe^{3+}) causes a colourless glass [34]. Therefore, it can be deduced that the colouring effect of iron may depend significantly on the composition of the glass as a function of the coordination environment of iron ions in the glass structure [34,35]. For instance, Fe^{2+} in six-coordinate turns the glass to a bluish-green or dark blue colour, whilst Fe^{3+} in low coordination imparts a yellow–green tint [35]. Similarly, it is informed that the chemical environment of the

Table 2
The compositions of pigment grain and the reaction layer determined by using EELS analysis.

	Elements (at.%)				Composition
	Zn	Fe	Cr	O	
Pigment (1)	–	1.97 ± 0.07	1.00 ± 0.18	4 ± 0.00	$Fe_{1.97}Cr_{1.00}O_4$
Reaction layer (2)	0.37 ± 0.04	1.04 ± 0.08	1.04 ± 0.14	4 ± 0.00	$Zn_{0.37}Fe_{1.04}Cr_{1.04}O_4$
Reaction layer (3)	0.34 ± 0.06	0.64 ± 0.11	1.38 ± 0.18	4 ± 0.00	$Zn_{0.34}Fe_{0.64}Cr_{1.38}O_4$
Reaction layer (4)	0.42 ± 0.04	1.02 ± 0.16	1.17 ± 0.18	4 ± 0.00	$Zn_{0.42}Fe_{1.02}Cr_{1.17}O_4$
Reaction layer (5)	0.43 ± 0.06	0.59 ± 0.11	1.52 ± 0.21	4 ± 0.00	$Zn_{0.43}Fe_{0.59}Cr_{1.52}O_4$
Reaction layer (6)	0.56 ± 0.07	0.64 ± 0.07	1.36 ± 0.19	4 ± 0.00	$Zn_{0.56}Fe_{0.64}Cr_{1.36}O_4$
Reaction layer (7)	0.60 ± 0.06	0.77 ± 0.24	1.40 ± 0.30	4 ± 0.00	$Zn_{0.60}Fe_{0.77}Cr_{1.40}O_4$
Reaction layer (8)	0.66 ± 0.09	0.84 ± 0.26	1.37 ± 0.08	4 ± 0.00	$Zn_{0.66}Fe_{0.84}Cr_{1.37}O_4$
The average composition of reaction layer	0.48 ± 0.12	0.79 ± 0.18	1.32 ± 0.16	4 ± 0.00	$Zn_{0.48}Fe_{0.79}Cr_{1.32}O_4$

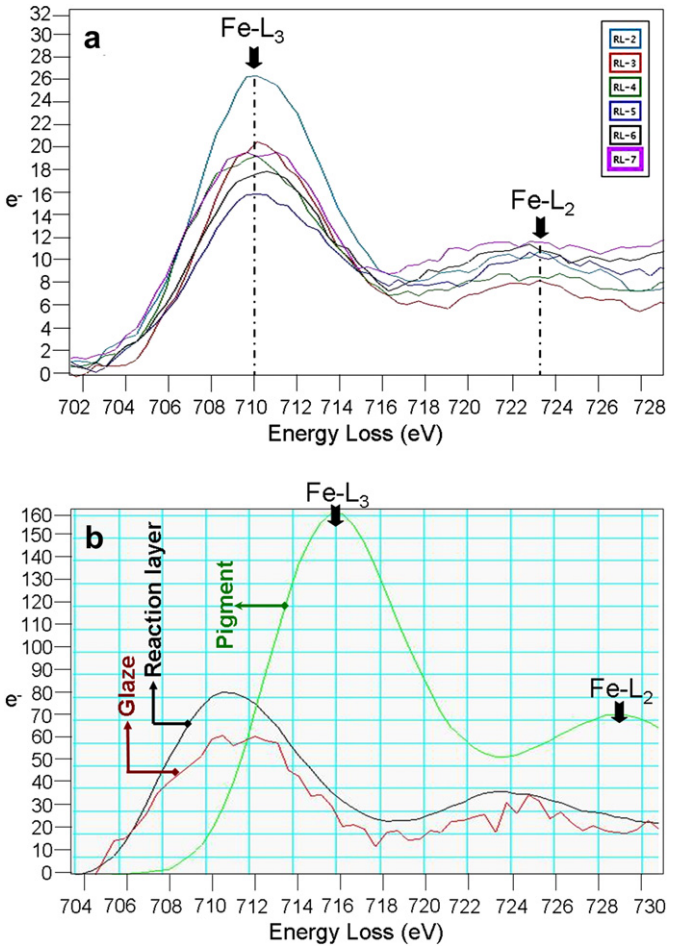

Fig. 9. (a) The comparison of Fe-$L_{3,2}$ edges acquired from all the grains existing in the reaction layer (RL-numbers show the grains marked in the Fig. 4(b)) and (b) the comparative EEL spectra demonstrating the detailed view of Fe-L_3 and Fe-L_2 edges corresponding to the pigment, grain RL-7 from the reaction layer and the glaze.

iron in a matured simple feldspathic glaze plays a key role on the evolution of colouring [36]. More interestingly, depending on the iron's specific atomic position and its valance state in a crystal structure, the attainable colour considerably varies resulting in a rather different than expected [34]. In such an example, aquamarine is beryl, just as is the emerald, but its colour is derived from iron [34]. When iron is present in one site in the crystal, a blue colour is resulted [34]. But, when iron is present in another site, the colour depends on the valance state: Fe^{3+} gives a yellow, while Fe^{2+} results in colourless appearance [34]. Considering all these reasons, the observation of Fe^{2+} in the both reaction layer and ZnO-containing glaze as different from the Fe^{3+} in the pigment grain can probably be the reason of the undesirable brown colour in this system.

4. Conclusions

With the use of FIB technique, a thin sample for analytical TEM analysis was successfully produced from a specifically selected area between a pigment grain and glaze in a very brittle glaze matrix. Analytical TEM observations on the FIBed sample showed a formation of a distinct reaction layer between Fe–Cr black pigment and ZnO-containing glaze. The reaction layer was composed of individual grains formed as a result of interactive diffusion. Zn diffused to the pigment side whilst Cr and Fe diffused from the pigment grain and reacted to generate the reaction layer. The average composition of the reaction layer was calculated as $Zn_{0.48}Fe_{0.79}Cr_{1.32}O_4$ by using quantitative EELS analysis. It was also observed that Fe diffused into the glaze region. The comparative EELS analysis showed that the oxidation state of Fe ion was 3+ in the pigment grain, whereas it was changed to 2+ in the reaction layer and the glaze. Therefore, it was concluded that the valence variation of Fe, the formation of $Zn_{0.48}Fe_{0.79}Cr_{1.32}O_4$ compound and the outward diffusion of Fe into the glaze were the key factors for the colour change in Fe–Cr pigment in the ZnO-containing glaze. Considering the results presented here, we anticipate that the concept of preparing a TEM sample from brittle materials like glasses through FIB technique will also be useful model study to understand the possible interactions taking place between pigments and glazes and/or crystals and glazes in many kind of systems.

Acknowledgements

We would like to thank Bilkent University UNAM laboratories for TEM sample preparation with FIB. One of us (H. Yurdakul) also would like to express his gratitude to Dr. A.R. Lupini at Oak Ridge National Laboratory (ORNL) for the fruitful discussion and helps about the STEM-SI data set.

References

[1] Hajjaji W, Seabra MP, Labrincha JA. Evaluation of metal-ions containing sludges in the preparation of black inorganic pigments. Journal of Hazardous Materials 2011;185(2–3):619–25.
[2] Camara B. Inorganic black pigments containing molybdenum. European Patent Specification; 2003, EP 1 098 938 B1.
[3] Costa G, Della VP, Ribeiro MJ, Oliveria APN, Monros G, Labrincha JA. Synthesis of black ceramic pigments from secondary raw materials. Dyes and Pigments 2008;77:137–44.
[4] Ozel E, Turan S. Production and characterisation of iron-chromium pigments and their interactions with transparent glazes. Journal of the European Ceramic Society 2003;23:2097–104.
[5] Ozel E, Unluturk G, Turan S. Production of brown pigments for porcelain insulator applications. Journal of the European Ceramic Society 2006;26:735–40.
[6] Shen L, Qiao Y, Guo Y, Tan J. Preparation of nanometer-sized black iron oxide pigment by recycling of blast furnace flue dust. Journal of Hazardous Materials 2010;177:495–500.
[7] Escardino A, Mestre S, Barba A, Beltran V, Blasco A. Synthesis mechanism of a iron-chromium ceramic pigment. Journal of the American Ceramic Society 2000;83:29–32.
[8] Escardino A, Mestre S, Barba A, Beltran V, Blasco A. Kinetic study of black Fe_2O_3-Cr_2O_3 pigment synthesis: I, influence of synthesis time and temperature. Journal of the American Ceramic Society 2003;86:945–50.
[9] ALy MH, Ismael IS, Bondioli F. Synthesis of coloured ceramic pigments by using chromite and manganese ores mixtures. Cerâmica 2010;56:156–61.
[10] Milanez KW, Kuhnen NC, Riella HG, Kniess CT. Obtainment of ceramics pigments (Fe, Zn)Cr_2O_4 using waste of electroplating as raw material. Materials Science Forum 2005;498–499:654–7.
[11] Yang GQ, Han B, Sun ZT, Yan LM, Wang XY. Preparation and characterization of brown nanometer pigment with spinel structure. Dyes and Pigments 2002;55:9–16.
[12] Robbins M, Wertheim GK, Sherwood RC, Buchanan DNE. Magnetic properties and site distributions in the system $FeCr_2O_4$-Fe_3O_4($Fe^{2+}Cr_{2-x}Fe_x^{3+}O_4$). Journal of Physics and Chemistry of Solids 1971;32:717–29.
[13] Colour, pigments and colouring in ceramics. Modena, Italy: S.A.L.A. srl; 2003. p. 60.
[14] Ozel E, Yurdakul H, Turan S, Ardit M, Cruciani G, Dondi M. Co-doped willemite ceramic pigments: technological behaviour, crystal structure and optical properties. Journal of the European Ceramic Society 2010;30:3319–29.
[15] Ahmadi S, Aghaei A, Yekta BE. Synthesis of Y(Al, Cr)O_3 red pigments by co-precipitation method and their interactions with glazes. Ceramics International 2009;35:3485–8.
[16] Bernardin AM. Diffusion of Cr–Fe–Al–Zn pigment in a zirconia glaze. Dyes and Pigments 2008;79:54–8.
[17] Lavat AE, Wagner CC, Tasca JE. Interaction of Co-ZnO pigments with ceramic frits: a combined study by XRD, FTIR and UV-visible. Ceramics International 2008;34:2147–53.
[18] Eppler RA, Eppler DR. Glazes and glass coatings. Westerville: American Ceramic Society; 2000.

[19] Eppler DR, Eppler RA. On the relative stability of ceramic pigments. Ceramic Engineering and Science Proceedings 1997;18:139–49.
[20] Murdock SH, Eppler RA. The interaction of ceramic pigments with glazes. American Ceramic Society Bulletin 1989;68:77–8.
[21] Williams DB, Watanabe M, Papworth AJ, Li JC. Quantitative characterization of the composition, thickness and orientation of thin films in the analytical electron microscope. Thin Solid Films 2003;424:50–5.
[22] Egerton RF. Electron energy-loss spectroscopy in the electron microscope. 2nd ed. New York: Plenum Press; 1996.
[23] Kyser DF, Murata K. Quantitative electron microprobe analysis of thin films on substrates. IBM Journal of Research and Development 1974;18: 352–63.
[24] Pennycook SJ, Varela M, Chisholm MF, Borisevich AY, Lupini AR, Van Benthem K, et al. Scanning transmission electron microscopy of nanostructures. In: Narlikar AV, Fu YY, editors. The Oxford handbook of nanoscience and technology. Materials, vol. II. UK: Oxford University Press; 2010. p. 205–44.
[25] Spinelli A, Novaes de Oliveira AP. Synthesis of heteromorphic iron oxide red pigment for ceramic application. Qualicer Spain; 2002:245–8.
[26] Calbo J, Garcia A, Sorli S, Tena MA, Ros LJ, Monros G. Waste prevention plan in the ceramic industry: decrease in level of hazard as reduction indicator. Qualicer Spain; 2002:147–57.
[27] Van Vlack LH. Physical ceramics for engineers. London: Addison-Wesley; 1964.
[28] Kingery WD, Bowen HK, Uhlmann DR. Introduction to ceramics. 2nd ed. New York: John Wiley & Sons; 1976.
[29] Okamoto JK, Pearson DH, Hightower A, Ahn CC, Fultz B. EELS analysis of the electronic structure and microstructure of metals. In: Ahn CC, editor. Transmission electron energy loss spectroscopy in materials science and the EELS ATLAS. USA: Wiley-VCH Verlag GmbH & Co., KGaA; 2004. p. 317–52.
[30] Gloter A, Zbinden M, Guyot F, Gaill F, Colliex C. TEM-EELS study of natural ferrihydrite from geological-biological interactions in hydrothermal systems. Earth and Planetary Science Letters 2004;222:947–57.
[31] Schmid HK, Mader W. Oxidation states of Mn and Fe in various compound oxide systems. Micron 2006;37:426–32.
[32] Van Aken PA, Liebscher B, Styrsa VJ. Quantitative determination of iron oxidation states in minerals using Fe $L_{2,3}$-edge electron energy-loss near-edge structure spectroscopy. Physics and Chemistry of Minerals 1998;25:323–7.
[33] Hamer F, Hamer J. The potter's dictionary of materials and techniques. 5th ed. London: A & C Black Publishers Ltd; 2004.
[34] Nassau K. The physics and chemistry of color, the fifteen causes of color. 2nd ed. John Wiley & Sons Inc.; 2001.
[35] Radchenko YS, Levitskii IA, Ugolev II. Investigation of glasses and glaze coats of composition R_2O-RO-Fe_2O_3(FeO)-Al_2O_3-B_2O_3-SiO_2 by the EPR method. Journal of Applied Spectroscopy 2003;70:821–6.
[36] Ali NJ, Gillespie PA, Mcwhinnie WR. The chemistry of simple ceramic glazes-I. ^{57}Fe Mössbauer studies of iron-containing glazes and glasses. Polyhedron 1990;9:999–1007.